SCIENCE CHINA
Technological Sciences

•Article•

March 2020 Vol.63 No.3: 397–409
https://doi.org/10.1007/s11431-019-9552-6

Chassis integrated control for 4WIS distributed drive EVs with model predictive control based on the UKF observer

SONG YiTong, SHU HongYu* & CHEN XianBao

State Key Laboratory of Mechanical Transmissions, Chongqing University, Chongqing 400044, China

Received April 1, 2019; accepted June 28, 2019; published online August 19, 2019

Four-wheel independent steering (4WIS) system and direct yaw moment control (DYC) have an important influence on vehicle lateral stability. However, DYC has a great effect on the longitudinal velocity, and the capability of 4WIS is limited to stability. To decrease the influence on the longitudinal velocity and improve the stability of electrical vehicles, a chassis controller integrated with a 4WIS system and a DYC system with model predictive control (MPC) is designed. The framework consists of an unscented Kalman filter (UKF) observer and an MPC that contains three blocks: supervisor blocks, upper blocks and lower blocks. First, the sideslip angle, longitudinal velocity and lateral tire forces are estimated by the UKF observer; second, a bicycle model is utilized in the supervisor to calculate the desired values; third, the upper blocks are designed with the MPC to optimize the target steering angles and longitudinal tire forces under the constraints of subsystems; to facilitate the design of the MPC, a nonlinear tire is simplified based on the Taylor expansion method; finally, the target steering angles and longitudinal tire forces are achieved by the lower blocks. The integrated controller is simulated on the co-simulation platform of MATLAB-Carsim. The results show that the proposed integrated controller has less impact on longitudinal velocity and could effectively improve vehicle stability.

unscented Kalman filter, model predictive control, Taylor expansion, integrated controller

Citation: Song Y T, Shu H Y, Chen X B. Chassis integrated control for 4WIS distributed drive EVs with model predictive control based on the UKF observer. Sci China Tech Sci, 2020, 63: 397–409, https://doi.org/10.1007/s11431-019-9552-6

1 Introduction

As a part of a vehicle's active safety system, electronic stability control (ESC) has attracted wide interest in research for a long time [1,2]. With the development of vehicle electronic technologies, there are increasing types of advanced technologies applied to ESCs, such as differential braking, active front steering (AFS), active roll system (ARS) and direct yaw-moment control (DYC). All of these advanced technologies can improve vehicle lateral stability [3–5]. Numerous studies [1,4,6–8] have examined the handling and stability of vehicles with DYC.

To simultaneously control the yaw rate and sideslip angle, chassis-integrated control, which could enhance vehicle lateral stability, has been studied by researchers in recent years. Wu et al. [9] presented a hierarchical controller of AFS and DYC with model predictive control (MPC) for vehicle dynamic stability. Zhang et al. [10] researched a hierarchical controller with a combination of AFS and DYC on the basis of a slip ratio estimation for vehicle dynamic stability. Her et al. [11,12] proposed an integrated controller with ESC, four-wheel drive (4WD) and ARS to enhance the vehicle lateral performance. Cheng et al. [13] proposed a hierarchical structure controller for autonomous vehicles based on the MPC theory, improving vehicle stability and driving comfort as well as maintaining performance. Yang et al. [14] proposed an integrated controller based on a linear quadratic regulator (LQR) considering the tire cornering stiffness. Meng et al. [15] designed a hierarchical structure controller with AFS and DYC based on a non-smooth control method

*Corresponding author (email: shycqu@163.com)

considering an uncertain disturbance. Shuai et al. [16] proposed a controller based on LQR considering time delays to decrease the influence of time-varying delays of AFS and DYC. Fan and Zhao [17] designed an integrated controller-coordinated AFS/ESC system and improved vehicle stability and safety. Several researchers [3,18,19] proposed MPC controllers to improve stability and track the desired path.

The integrated controllers mentioned above are designed to improve the lateral stability of a vehicle to a certain extent. However, some state parameters (e.g., longitudinal velocity, lateral tire forces and sideslip angle) are unmeasured variables. In addition, it is meaningful to emphasize that longitudinal velocity, lateral tire forces and sideslip angle are the significant vectors affecting vehicle handling and stability performance. Therefore, many studies have researched the design of vehicle state observers.

Baffet et al. [20,21] designed an observer for the lateral tire forces using an extended Kalman filter (EKF) and slide model control theory. Jin and Yin [22] estimated the lateral tire forces and sideslip angle using a dual unscented Kalman filter (UKF) observer. However, the variables mentioned above were estimated assuming that the lateral tire forces on both sides are the same. In fact, the sprung mass of each wheel will be redistributed, and the lateral tire forces of the four wheels are different when the vehicle turns. Therefore, extensive research has been conducted considering the different tire performances on both sides, which are influenced by lateral load transfer. Several researchers [23,24] estimated the lateral tire forces and sideslip angle based on an interactive UKF observer; Cheng et al. [25] designed an adaptive unified sliding mode observer and mode-switch observer to estimate the tire forces and road friction coefficient, respectively; Cheng et al. [26] estimated the sideslip angle with an adaptive square-root cubature Kalman filter considering the unknown noises of sensors. However, most studies have investigated the observation of lateral forces and sideslip angle while ignoring the longitudinal velocity. The longitudinal velocity is also difficult to measure.

In addition, according to our previous research [23], we found that the DYC controller has an obvious effect on yaw rate, while DYC has a weak effect on sideslip angle and always leads to a rapid drop in the longitudinal velocity. This phenomenon occurs not only in our research but also in all DYC control systems. Therefore, considering that parameters such as lateral tire forces, longitudinal velocity and vehicle sideslip angle are rarely measured accurately, and MPC is robust and has been increasingly implemented on vehicles [27], this study begins with the design of a UKF observer and then designs an integrated controller based on the estimated parameters from the UKF to enhance vehicle stability. The main contributions or improvements of this paper include the design of UKF observers, the design of integrated controllers, and the simplification of nonlinear tires. The details are as follows.

(1) Design of the UKF observer: considering the different tire performances on both sides, which are influenced by the lateral load transfer, the longitudinal velocity and lateral tire forces are estimated, as well as the sideslip angle, with the UKF method based on the measurable variables. Therefore, the observer could provide accurate values for the integrated controller.

(2) Design of the integrated controller: considering that the capacity of 4WIS is limited to the vehicle lateral stability and that the problem of the longitudinal velocity is decreased by DYC, reducing the longitudinal dynamic performance, it is significant to develop the effect of each subsystem. The integrated MPC of 4WIS and DYC is designed to optimize the target steering angles and longitudinal tire forces based on the estimated parameters, improving the vehicle stability and reducing influence on the characteristics of longitudinal dynamics.

(3) Simplification of nonlinear tire: considering the magic formula (MF) tire has highly nonlinearity and is difficult for the design of the MPC, this paper conducts a method to simplify the MF tire based on the Taylor expansion method, not only retaining the nonlinear tire characteristics but also facilitating the design of the MPC.

2 Vehicle dynamics model

2.1 Nonlinear vehicle model

Some appropriate simplifications are made in the present paper: (1) ignoring the vertical motion; (2) ignoring the pitch motion; (3) ignoring the air resistance and rolling resistance of the wheels; and (4) assuming that the road surface is flat. A 7-DOF vehicle model that contains nonlinear dynamic characteristics is used, as shown in Figure 1.

Longitudinal motion:

$$m\left(\frac{\mathrm{d}v_x}{\mathrm{d}t}-v_y w_r\right)=\left(F_{xfl}+F_{xfr}\right)\cos\delta_f-\left(F_{yfl}+F_{yfr}\right)\sin\delta_f +(F_{xrl}+F_{xrr})\cos\delta_r-\left(F_{yrl}+F_{yrr}\right)\sin\delta_r; \quad (1)$$

Lateral motion:

$$mv_x\left(\frac{\mathrm{d}\beta}{\mathrm{d}t}+w_r\right)=\left(F_{xfl}+F_{xfr}\right)\sin\delta_f+\left(F_{yfl}+F_{yfr}\right)\cos\delta_f +(F_{xrl}+F_{xrr})\sin\delta_r+\left(F_{yrl}+F_{yrr}\right)\cos\delta_r; \quad (2)$$

Yaw motion:

$$\begin{aligned}I_{zz}\frac{\mathrm{d}w_r}{\mathrm{d}t}=&a\left(F_{xfl}+F_{xfr}\right)\sin\delta_f+a\left(F_{yfl}+F_{yfr}\right)\cos\delta_f\\&+0.5t_f\left(F_{xfr}-F_{xfl}\right)\cos\delta_f+0.5t_f\left(F_{yfl}-F_{yfr}\right)\sin\delta_f\\&-b(F_{xrl}+F_{xrr})\sin\delta_r-b\left(F_{yrl}+F_{yrr}\right)\cos\delta_r\\&+0.5t_r(F_{xrr}-F_{xrl})\cos\delta_r+0.5t_r\left(F_{yrl}-F_{yrr}\right)\sin\delta_r. \quad (3)\end{aligned}$$

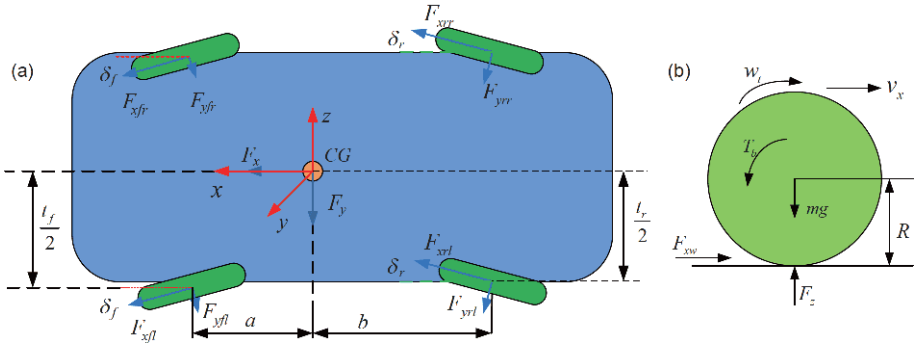

Figure 1 (Color online) 7-DOF vehicle model. (a) Nonlinear vehicle model; (b) wheel dynamics model.

The rotation equation of the four wheels is as follows:

$$I_w \frac{\mathrm{d}w_{tij}}{\mathrm{d}t} = T_{tij} - T_{bij} - F_{xij}R, \tag{4}$$

where v_x and v_y individually represent the longitudinal and lateral velocities, m denotes the vehicle mass, w_r and β are the yaw rate and sideslip angle, F_{xij} and F_{yij} are the longitudinal and lateral tire forces, respectively, δ_f and δ_r are the front and rear steering angles, respectively, a and b are the distance from the gravity center of the mass to the front and rear axles, t_f and t_r are the track width of the front and rear axils, I_{zz} is the yaw inertia moment, I_w is the wheel inertia moment, w_{ti} is the wheel angular velocity, T_{tij} and T_{bij} are the inputs of driving and braking torques of each wheel, and R is the radius of each wheel.

2.2 Reference values calculation model

The bicycle model, considered as a reference, is employed here to calculate the desired state vectors. The bicycle dynamics model is presented in Figure 2.

The bicycle model can be described as follows:

$$\begin{pmatrix} \frac{\mathrm{d}\beta}{\mathrm{d}t} \\ \frac{\mathrm{d}w_r}{\mathrm{d}t} \end{pmatrix} = \begin{bmatrix} \frac{2k_f+2k_r}{mv_x} & \frac{2ak_f-2bk_r}{mv_x^2} - 1 \\ \frac{2ak_f-2bk_r}{I_{zz}} & \frac{2a^2k_f+2b^2k_r}{I_{zz}v_x} \end{bmatrix} \begin{pmatrix} \beta \\ w_r \end{pmatrix} + \begin{bmatrix} \frac{-2k_f}{mv_x} \\ \frac{-2ak_f}{I_{zz}} \end{bmatrix} \delta, \tag{5}$$

where k_f and k_r individually represent the cornering stiffness of the front and rear wheels, and δ is the steering angle input.

2.3 MF tire model

The MF tire model [28] is a well-known tire model that is a semi-empirical formula with triangular function combination and could describe the characteristics of tires in the nonlinear region. The tire forces can be shown as follows:

$$F = D\sin\{C\arctan[Bx - E(Bx - \arctan(Bx))]\}, \tag{6}$$

where x represents the longitudinal wheel slip and lateral slip angle of the tires.

In addition, the lateral slip angle could be calculated as

$$\begin{aligned} \alpha_f &= \delta_f - \arctan\left(\frac{v_y + aw_r}{v_x}\right), \\ \alpha_r &= \delta_r - \arctan\left(\frac{-v_y + bw_r}{v_x}\right). \end{aligned} \tag{7}$$

Moreover, the longitudinal wheel slip could be calculated by the following equation:

$$\kappa_i = \begin{cases} \frac{v_x - Rw_t}{v_x}, & v_x \geq Rw_t. \\ \frac{Rw_t - v_x}{Rw_t}, & Rw_t > v_x. \end{cases} \tag{8}$$

The sprung mass will be redistributed when the vehicle turns, and the vertical load of each wheel can be calculated by the equation as

$$F_{zi} = mg\Pi_i + ma_x\Gamma_i + ma_y\Xi_i + ma_xa_y\Omega_i, \tag{9}$$

where $\Pi_{1,2} = \frac{b}{2(a+b)}$, $\Pi_{3,4} = \frac{a}{2(a+b)}$, $\Gamma_{1,2} = -\frac{h}{2(a+b)}$, $\Gamma_{3,4} = \frac{h}{2(a+b)}$, $\Xi_1 = -b\frac{h}{(a+b)t_f}$, $\Xi_2 = b\frac{h}{(a+b)t_f}$, $\Xi_3 = -a\frac{h}{(a+b)t_r}$, $\Xi_4 = a\frac{h}{(a+b)t_r}$, $\Omega_{1,3} = \frac{h^2}{g(a+b)t_f}$, $\Omega_{2,4} = -\frac{h^2}{g(a+b)t_f}$.

3 Design of state observer

3.1 UKF observer

Recently, the Kalman filter, Luenberger method, sliding mode method and fuzzy theory have been applied to the design of state observers, particularly state observers de-

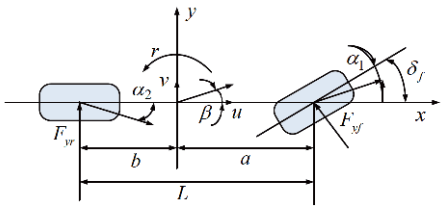

Figure 2 Bicycle dynamics model.

signed based on the EKF. However, for a highly nonlinear system, the UKF has many advantages [29] compared with the EKF. In this paper, an observer that can estimate the longitudinal velocity and sideslip angle as well as lateral tire forces is designed on the basis of the UKF theory by utilizing the measurements, considering the nonlinear characteristics of the vehicle model. The UKF algorithm for each single filter can be found in ref. [23], and no further elaboration about the principle of the UKF algorithm will be made in this article.

As this stage, the tire forces should be extended to the state vector for the estimation. Therefore, the system vector in the present state is shown as eq. (10) based on the nonlinear vehicle model.

$$\mathbf{x}=\begin{bmatrix} v_x,\beta,w_r,w_{tfl},w_{tfr},w_{trl},w_{trr},F_{xfl},F_{xfr},\\ F_{xrl},F_{xrr},F_{yfl},F_{yfr},F_{yrl},F_{yrr}\end{bmatrix}^{\mathrm{T}}. \tag{10}$$

The measurement and estimable variables are shown as follows:

$$\begin{aligned}&\mathbf{z}=[a_x,a_y,w_r,w_{tfl},w_{tfr},w_{trl},w_{trr}]^{\mathrm{T}},\\ &\mathbf{x}_{\text{estimated}}=\left[v_x,\beta,F_{yfl},F_{yfr},F_{yrl},F_{yrr}\right]^{\mathrm{T}}.\end{aligned} \tag{11}$$

The inputs of the vehicle model are defined as

$$\mathbf{u}=\left[\delta_f,\delta_r,T_{tfl},T_{tfr},T_{trl},T_{trr},T_{bfl},T_{bfr},T_{brl},T_{brr}\right]^{\mathrm{T}}. \tag{12}$$

The nonlinear function can be calculated as follows:

$$\begin{aligned}\frac{\mathrm{d}\mathbf{x}}{\mathrm{d}t}&=f(\mathbf{x},\mathbf{u})\\ &=\begin{bmatrix} f_1(\mathbf{x},\mathbf{u}),f_2(\mathbf{x},\mathbf{u}),f_3(\mathbf{x},\mathbf{u}),f_4(\mathbf{x},\mathbf{u}),\\ f_5(\mathbf{x},\mathbf{u}),f_6(\mathbf{x},\mathbf{u}),f_7(\mathbf{x},\mathbf{u}),f_8(\mathbf{x},\mathbf{u}),\\ f_9(\mathbf{x},\mathbf{u}),f_{10}(\mathbf{x},\mathbf{u}),f_{11}(\mathbf{x},\mathbf{u}),f_{12}(\mathbf{x},\mathbf{u}),\\ f_{13}(\mathbf{x},\mathbf{u}),f_{14}(\mathbf{x},\mathbf{u}),f_{15}(\mathbf{x},\mathbf{u})\end{bmatrix}^{\mathrm{T}},\end{aligned} \tag{13}$$

where

$$f_1(\mathbf{x},\mathbf{u})=\frac{1}{m}\begin{pmatrix}(F_{xfl}+F_{xfr})\cos\delta_f-(F_{yfl}+F_{yfr})\sin\delta_f\\ +(F_{xrl}+F_{xrr})\cos\delta_r-(F_{yrl}+F_{yrr})\sin\delta_r\end{pmatrix}+v_y w_r,$$

$$f_2(\mathbf{x},\mathbf{u})=\frac{1}{mv_x}\begin{pmatrix}(F_{xfl}+F_{xfr})\sin\delta_f+(F_{yfl}+F_{yfr})\cos\delta_f\\ +(F_{xrl}+F_{xrr})\sin\delta_r+(F_{yrl}+F_{yrr})\cos\delta_r\end{pmatrix}-w_r,$$

$$f_3(\mathbf{x},\mathbf{u})=\frac{1}{I_{zz}}\begin{pmatrix}a(F_{xfl}+F_{xfr})\sin\delta_f+a(F_{yfl}+F_{yfr})\cos\delta_f\\ +0.5t_f(F_{xfr}-F_{xfl})\cos\delta_f+0.5t_f(F_{yfl}-F_{yfr})\sin\delta_f\\ -b(F_{xrl}+F_{xrr})\sin\delta_r-b(F_{yrl}+F_{yrr})\cos\delta_r\\ +0.5t_r(F_{xrr}-F_{xrl})\cos\delta_r+0.5t_r(F_{yrl}-F_{yrr})\sin\delta_r\end{pmatrix},$$

$$f_m(\mathbf{x},\mathbf{u})=\left(T_{tij}-T_{bij}-F_{xij}R\right)/I_{wij},$$

$$f_p(\mathbf{x},\mathbf{u})=0,$$

$$f_q(\mathbf{x},\mathbf{u})=0,$$

where ij=*fl*, *fr*, *rl*, *rr*; m=4, 5, 6, 7; p=8, 9, 10, 11; q=12, 13, 14, 15.

For the design of the UKF observer, eq. (13) should be reduced to the form of eq. (14). The Euler discrete method is applied in this paper, and the discrete system function can be described as

$$\mathbf{x}_{k+1}=E(\mathbf{x},\mathbf{u})=\mathbf{x}_k+\Delta T f(\mathbf{x},\mathbf{u}), \tag{14}$$

where ΔT represents sample time.

The particular observation is derived as follows:

$$\mathbf{z}=h(\mathbf{x},\mathbf{u})=\begin{bmatrix}h_1(\mathbf{x},\mathbf{u}),h_2(\mathbf{x},\mathbf{u}),\\ h_3(\mathbf{x},\mathbf{u}),h_{4ij}(\mathbf{x},\mathbf{u})\end{bmatrix}^{\mathrm{T}}, \tag{15}$$

where

$$h_1(\mathbf{x},\mathbf{u})=\frac{1}{m}\begin{pmatrix}(F_{xfl}+F_{xfr})\cos\delta_f-(F_{yfl}+F_{yfr})\sin\delta_f\\ +(F_{xrl}+F_{xrr})\cos\delta_r-(F_{yrl}+F_{yrr})\sin\delta_r\end{pmatrix},$$

$$h_2(\mathbf{x},\mathbf{u})=\frac{1}{m}\begin{pmatrix}(F_{xfl}+F_{xfr})\sin\delta_f+(F_{yfl}+F_{yfr})\cos\delta_f\\ +(F_{xrl}+F_{xrr})\sin\delta_r+(F_{yrl}+F_{yrr})\cos\delta_r\end{pmatrix},$$

$$h_3(\mathbf{x},\mathbf{u})=w_r,$$

$$h_{4ij}(\mathbf{x},\mathbf{u})=w_{tij},$$

where ij=*fl*, *fr*, *rl*, *rr*.

3.2 Simulation and analysis

In this section, the UKF observer is simulated in the MATLAB/Simulink platform to test the effectiveness and robustness of the observer. Two different driving conditions are selected in this paper. The simulation parameters are listed in Table 1. The initial condition is defined as follows: the initial longitudinal velocity is 33.48 km/h, there is no driving and braking torque, and the front and rear steering angles are shown in Figure 3. The comparisons of actual and estimated values are displayed in Figures 4 and 5 under different road friction coefficients. In this paper, the processed noise covariance $\mathbf{Q}$=diag([1×10^{-4}; 1×10^{-4}; 8×10^{-5}; 1×10^{-4}; 1×10^{-4}; 1×10^{-4}; 1×10^{-4}; 1×10^{-6}; 1×10^{-6}; 1×10^{-6}; 1×10^{-6}; 1×10^{-5}; 1×10^{-5}; 1×10^{-5}; 1×10^{-5}]), and the measurement noise cov-

Table 1 Major vehicle parameters

Symbols	Parameters	Values
m	Vehicle mass	2037 kg
I_{zz}	Inertia of Z axis	2975 kg m^2
R_w	Radius of wheel	0.31 m
a	Distance from front axle to gravity center	1.35 m
b	Distance from rear axle to gravity center	1.65 m
t_f	Track of front wheels	1.695 m
t_r	Track of rear wheels	1.775 m

ariance **R**=diag([1×10^{-4}; 1×10^{-4}; 1×10^{-4}; 1×10^{-4}; 1×10^{-4}; 1×10^{-4}; 1×10^{-4}]).

As shown in Figures 4 and 5, the estimated longitudinal velocity, lateral tire force of each wheel and sideslip angle using the UKF observer could effectively track the actual values under individual driving conditions. Consequently, the determined UKF observer in the present study could estimate the longitudinal velocity, lateral tire forces and sideslip angle effectively and precisely under high or low road friction coefficient conditions, and it shows better robustness, providing accurate values for the design of the MPC. In addition, the UKF observer could filter the noise for measurable signals and estimate the unmeasurable signals accurately.

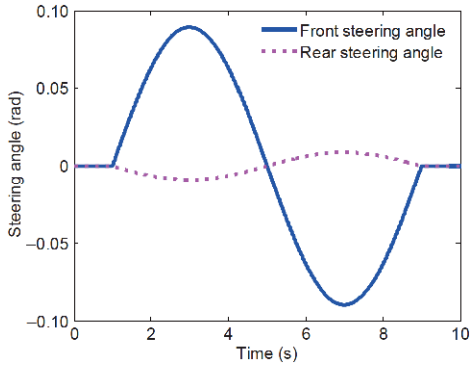

Figure 3 (Color online) Steering angle inputs of front and rear wheels.

In conclusion, the UKF observer could estimate the longitudinal velocity, lateral tire forces and sideslip angle effectively and precisely under high or low road friction coefficient conditions, and it shows better robustness.

4 Design of integrated controller with 4WIS and DYC

The scheme of the integrated controller with 4WIS and DYC in this paper is shown in Figure 6. As seen, the integrated controller is composed of three parts based on the UKF

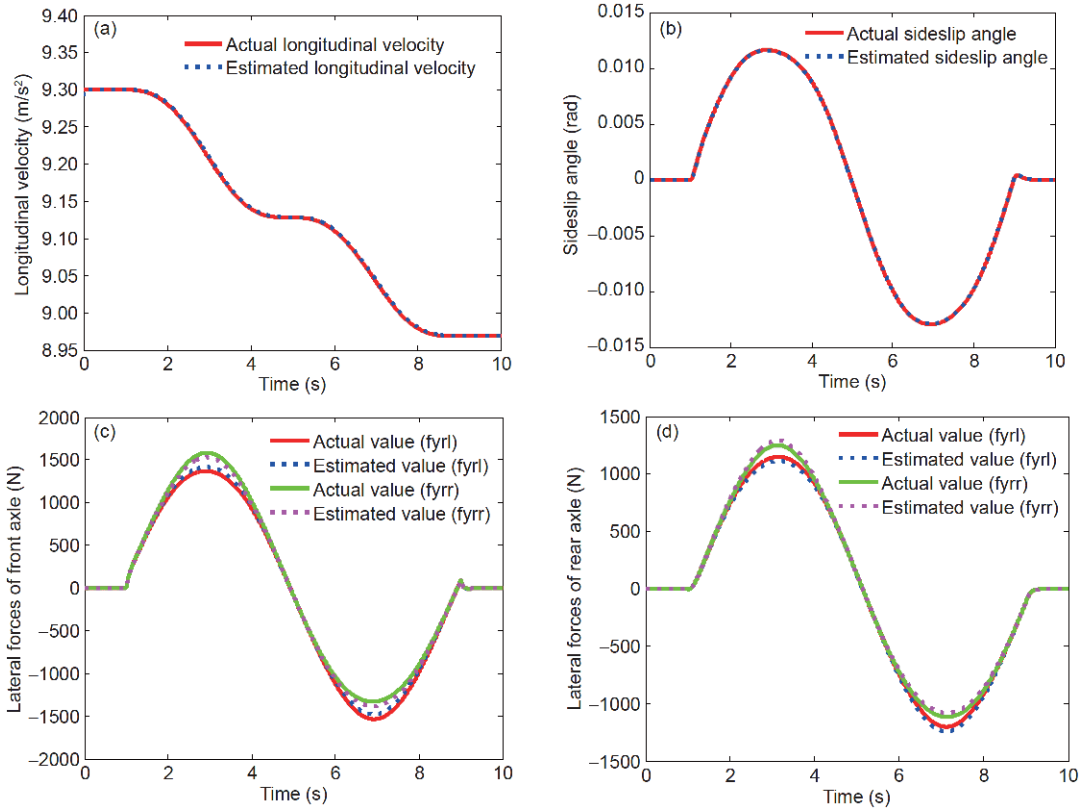

Figure 4 (Color online) Simulation results of actual and estimated values (road friction coefficient is 0.7). (a) Comparison of longitudinal velocity; (b) comparison of sideslip angle; (c) comparison of lateral tire forces of front axle; (d) comparison of lateral tire forces of rear axle.

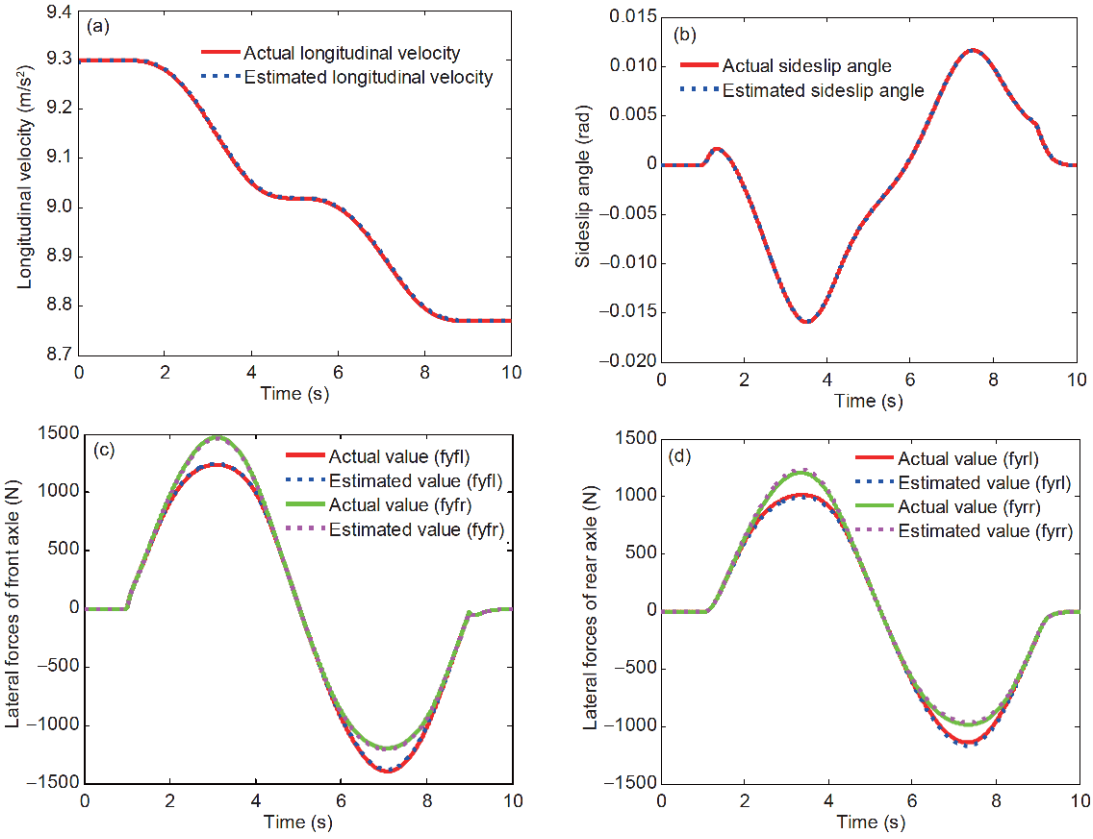

Figure 5 (Color online) Simulation results of actual and estimated values (road friction coefficient is 0.4). (a) Comparison of longitudinal velocity; (b) comparison of sideslip angle; (c) comparison of lateral tire forces of front axle; (d) comparison of lateral tire forces of rear axle.

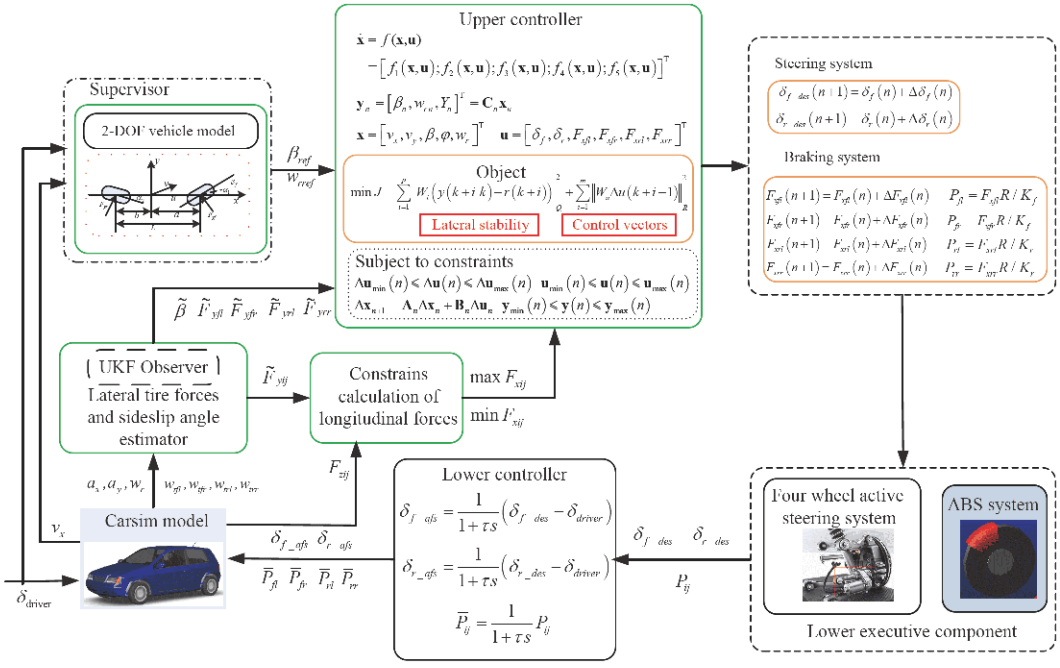

Figure 6 (Color online) Scheme of the integrated controller with 4WIS and DYC.

observer: the supervisor block, the upper block and the lower block.

In the supervisor module, according to the bicycle model, the target yaw rate is calculated along with the sideslip angle, providing the target values to the upper block; in the upper block module, the MPC integrated controller with 4WIS and

DYC is designed to optimize the target steering angles and longitudinal tire forces as the vehicle inputs to enhance the lateral vehicle stability, considering the constraints of control vector and actuators; in the lower block module, the target steering angles and longitudinal tire forces optimized by the upper controller are realized via the steering system and braking system.

4.1 Supervisor design

The supervisor is designed in line with the bicycle model to calculate the target values. In this paper, the desired states of a vehicle are defined as the sideslip angle and yaw rate and can be discretized based on eq. (5) with the Euler discrete method as follows:

$$\beta_d(n+1) = \beta_d(n) + T_s\frac{\mathrm{d}\beta_d(n)}{\mathrm{d}t}, \tag{16}$$

$$w_{rd}(n+1) = w_{rd}(n) + T_s\frac{\mathrm{d}w_{rd}(n)}{\mathrm{d}t}. \tag{17}$$

4.2 Upper level controller design

It is worth noting that the MF tire model is inconvenient for the design of the MPC, considering the real-time performance of the controller. Therefore, the MF tire model shown in eq. (6) is simplified based on the Taylor expansion method in this paper, retaining the nonlinear tire characteristics.

Differentiating the yields in eq. (6), the derivative of lateral forces can be obtained as

$$K_{ij}(n) = \partial F_{yij}(n) / \partial \alpha_{ij}(n). \tag{18}$$

For unified directions of state variables, eq. (18) can be shown as

$$\overline{K}_{ij} = -\frac{180}{\pi}\frac{\partial F_{yij}(n)}{\partial \alpha_{ij}(n)}. \tag{19}$$

The lateral tire forces at time n can be calculated by the lateral tire forces at $n-1$ based on the sideslip angles of tires at times n and $n-1$:

$$F_{yij}(n) = F_{yij}(n-1) + \overline{K}_{ij}\left(\alpha_{ij}(n) - \alpha_{ij}(n-1)\right). \tag{20}$$

The lateral tire forces calculated by eqs. (6) and (20) under different vertical loads (F_z=3, 5, 7 and 9 kN) are shown in Figure 7. The results show that the simplified model could effectively retain the nonlinear tire performance and track the lateral tire forces of the MF.

To track the desired yaw rate and sideslip angle, an upper block is designed based on the nonlinear vehicle model using the MPC theory. We define parameters, including longitudinal velocity, lateral forces and sideslip angle, estimated by the UKF observer as the inputs of the MPC. The state vector is defined as follows based on eqs. (1)–(3):

$$\mathbf{x} = \left[v_x, v_y, \beta, \varphi, w_r\right]^{\mathrm{T}}. \tag{21}$$

The control vectors of the MPC are the steering angles and longitudinal force of each wheel, assuming that the steering angles on both sides are the same. Therefore, the control vectors can be shown as follows:

$$\mathbf{u} = \left[\delta_f, \delta_r, F_{xfl}, F_{xfr}, F_{xrl}, F_{xrr}\right]^{\mathrm{T}}. \tag{22}$$

The state space model is defined as

$$\frac{\mathrm{d}\mathbf{x}}{\mathrm{d}t} = f(\mathbf{x},\mathbf{u}) = \begin{bmatrix} f_1(\mathbf{x},\mathbf{u}), f_2(\mathbf{x},\mathbf{u}), f_3(\mathbf{x},\mathbf{u}), \\ f_4(\mathbf{x},\mathbf{u}), f_5(\mathbf{x},\mathbf{u}) \end{bmatrix}^{\mathrm{T}}, \tag{23}$$

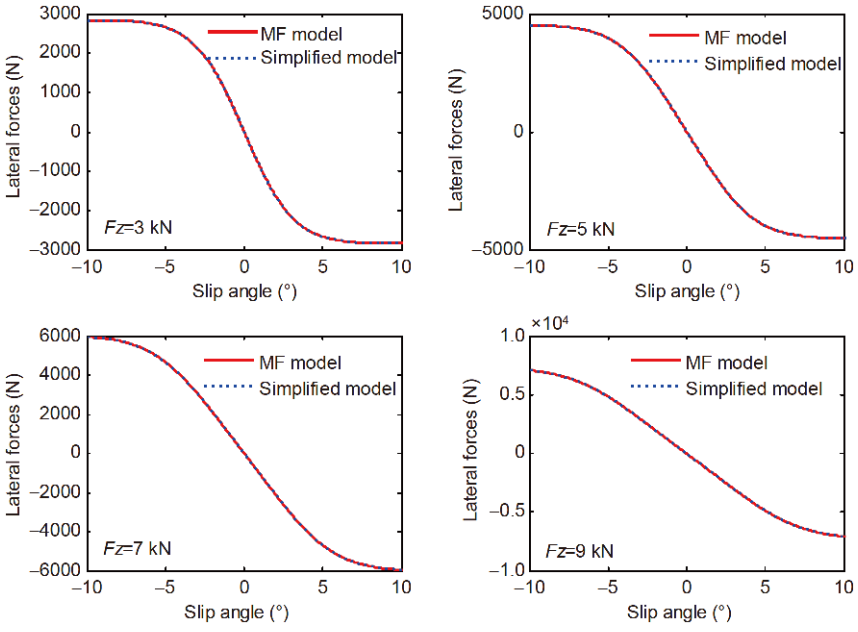

Figure 7 (Color online) Lateral tire forces under different vertical loads.

where

$$f_1(\mathbf{x},\mathbf{u}) = v_y(n)w_r(n) + \frac{1}{m}\begin{bmatrix}\left(F_{xfl}(n)+F_{xfr}(n)\right)\cos\delta_f(n) - \left(F_{yfl}+F_{yfr}(n)\right)\sin\delta_f(n)\\ +\left(F_{xrl}(n)+F_{xrr}(n)\right)\cos\delta_r(n) - \left(F_{yrl}(n)+F_{yrr}(n)\right)\sin\delta_r(n)\end{bmatrix},$$

$$f_2(\mathbf{x},\mathbf{u}) = -v_x(n)w_r(n) + \frac{1}{m}\begin{bmatrix}\left(F_{xfl}(n)+F_{xfr}(n)\right)\sin\delta_f(n) + \left(F_{yfl}(n)+F_{yfr}(n)\right)\cos\delta_f(n)\\ +\left(F_{xrl}(n)+F_{xrr}(n)\right)\sin\delta_r(n) + \left(F_{yrl}(n)+F_{yrr}(n)\right)\cos\delta_r(n)\end{bmatrix},$$

$$f_3(\mathbf{x},\mathbf{u}) = -w_r(n) + \frac{1}{mv_x(n)}\begin{bmatrix}\left(F_{xfl}(n)+F_{xfr}(n)\right)\sin\delta_f(n) + \left(F_{yfl}(n)+F_{yfr}(n)\right)\cos\delta_f(n)\\ +\left(F_{xrl}(n)+F_{xrr}(n)\right)\sin\delta_r(n) + \left(F_{yrl}(n)+F_{yrr}(n)\right)\cos\delta_r(n)\end{bmatrix},$$

$$f_4(\mathbf{x},\mathbf{u}) = w_r(n),$$

$$f_5(\mathbf{x},\mathbf{u}) = \frac{1}{I_{zz}}\begin{bmatrix}a\left(F_{xfl}(n)+F_{xfr}(n)\right)\sin\delta_f(n) + a\left(F_{yfl}(n)+F_{yfr}(n)\right)\cos\delta_f(n) + 0.5t_f\left(F_{xfr}(n)-F_{xfl}(n)\right)\cos\delta_f(n)\\ +0.5t_f\left(F_{yfl}(n)-F_{yfr}(n)\right)\sin\delta_f(n) - b\left(F_{xrl}(n)+F_{xrr}(n)\right)\sin\delta_r(n) - b\left(F_{yrl}(n)+F_{yrr}(n)\right)\cos\delta_r(n)\\ +0.5t_r\left(F_{xrr}(n)-F_{xrl}(n)\right)\cos\delta_r(n) + 0.5t_r\left(F_{yrl}(n)-F_{yrr}(n)\right)\sin\delta_r(n)\end{bmatrix}.$$

Discretizing eq. (23) can be expressed as

$$\Delta\mathbf{x}_{n+1} = \mathbf{A}_n\Delta\mathbf{x}_n + \mathbf{B}_n\Delta\mathbf{u}_n, \tag{24}$$

where $\mathbf{A}_n = \mathbf{I} + \Delta T\frac{\partial\mathbf{f}}{\partial\mathbf{x}}\Big|\mathbf{x}_n$, $\mathbf{B}_n = \Delta T\frac{\partial\mathbf{f}}{\partial\mathbf{u}}\Big|\mathbf{u}_n$, and ΔT represents sample time.

The measured system can be defined as follows:

$$\mathbf{y}_n = [\beta_n, w_{rn}]^{\mathrm{T}} = \mathbf{C}_n\mathbf{x}_n, \tag{25}$$

where $\mathbf{C}_n = \begin{bmatrix}0&0&1&0&0\\0&0&0&0&1\end{bmatrix}$.

Taking the limitation of steering and braking systems into account, the constraints of the control vectors are described as follows:

$$\mathbf{u}_{\min} \le \mathbf{u} \le \mathbf{u}_{\max}, \Delta\mathbf{u}_{\min} \le \Delta\mathbf{u} \le \Delta\mathbf{u}_{\max}, \tag{26}$$

where

$$\mathbf{u}_{\min} = \left[\delta_{f\min}, \delta_{r\min}, F_{xfl\min}, F_{xfr\min}, F_{xrl\min}, F_{xrr\min}\right]^{\mathrm{T}},$$

$$\mathbf{u}_{\max} = \left[\delta_{f\max}, \delta_{r\max}, F_{xfl\max}, F_{xfr\max}, F_{xrl\max}, F_{xrr\max}\right]^{\mathrm{T}},$$

$$\Delta\mathbf{u} = \left[\Delta\delta_f, \Delta\delta_r, \Delta F_{xfl}, \Delta F_{xfr}, \Delta F_{xrl}, \Delta F_{xrr}\right]^{\mathrm{T}},$$

$$\Delta\mathbf{u}_{\min} = \left[\Delta\delta_{f\min}, \Delta\delta_{r\min}, \Delta F_{xfl\min}, \Delta F_{xfr\min}, \Delta F_{xrl\min}, \Delta F_{xrr\min}\right]^{\mathrm{T}},$$

$$\Delta\mathbf{u}_{\max} = \left[\Delta\delta_{f\max}, \Delta\delta_{r\max}, \Delta F_{xfl\max}, \Delta F_{xfr\max}, \Delta F_{xrl\max}, \Delta F_{xrr\max}\right]^{\mathrm{T}},$$

where $\delta_{i\min}$ and $\delta_{i\max}$ individually represent the minimum and maximum steering angles of the front and rear wheels; $F_{xmn\min}$ and $F_{xmn\max}$ separately indicate the minimum and maximum longitudinal tire forces; $\Delta\delta_{i\min}$ and $\Delta\delta_{i\max}$ individually represent the minimum and maximum steering angle increments, respectively; $\Delta F_{xmn\min}$ and $\Delta F_{xmn\max}$ separately indicate the minimum and maximum increments of longitudinal tire forces, respectively, *i*=*f*, *r*, *mn*=*fl*, *fr*, *rl*, *rr*.

Considering the adhesion ellipse, the constraints of longitudinal tire forces F_{xij} are shown as follows:

$$F_{xij\min} = -\sqrt{\left(\mu F_{zij}\right)^2 - \left(\rho F_{yij}\right)^2}, \tag{27}$$

where ρ indicates the coefficient, and $\rho \le 1$.

The peak value of the yaw rate and sideslip angle yield [1,10] is

$$w_{r\_r} = 0.85\left|\frac{\mu g}{v_x}\right|\mathrm{sgn}(\delta), \quad \beta_r = \left|\arctan(0.02\mu g)\right|\mathrm{sgn}(\delta). \tag{28}$$

The MPC objective function in this paper is defined as follows:

$$J(\mathbf{x}(n),\Delta\mathbf{u}(n)) = \sum_{i=1}^{N_{\mathrm{p}}}\left\|\boldsymbol{\Gamma}_{dyn}(n+i|n) - \boldsymbol{\Gamma}_{dyn,ref}(n+i|n)\right\|_{\mathbf{Q}}^2 + \sum_{i=1}^{N_{\mathrm{c}}-1}\left\|\Delta\mathbf{u}_{dyn}(n+i|n)\right\|_{\mathbf{R}}^2 + \rho\varepsilon^2, \tag{29}$$

where $\mathbf{Q}$ and $\mathbf{R}$ individually represent the weight matrices of the controlled vectors of the MPC, and $\mathbf{Q} = \mathrm{diag}\left(W_\beta, W_{w_r}\right)$, $\mathbf{R} = \mathrm{diag}\left(W_{\delta_f}, W_{\delta_r}, W_{F_{xfl}}, W_{F_{xfr}}, W_{F_{xrl}}, W_{F_{xrr}}\right)$. $\boldsymbol{\Gamma}_{dyn}$ and $\boldsymbol{\Gamma}_{dyn,ref}$ individually represent the controlled outputs and reference outputs, respectively. N_{p} and N_{c} individually represent the prediction and control horizon, respectively, and $N_{\mathrm{p}} \ge N_{\mathrm{c}}$. ρ and ε individually represent the weight and slack factors. The first term represents the errors between the actual state and ideal state, and the second term represents the increment of the control vectors. The objective function minimizes the

errors of the actual state and ideal state and the increment of the control vectors.

Based on the objective function mentioned above, the problems of the MPC controller can be expressed as follows:

$$\min_{i=1:N_p} J(\mathbf{x}(n), \Delta\mathbf{u}(n)). \tag{30}$$

The constraints are expressed as follows:

$$\begin{aligned}
&\mathbf{x}_{n+1,t} = \mathbf{f}(\mathbf{x}_{n,t}, \mathbf{u}_{n,t}), \quad n = t, \ldots, t+H_p-1,\\
&\mathbf{u}_{n,t} = \mathbf{u}_{n-1,t} + \Delta\mathbf{u}_{n,t}, \quad n = t, \ldots, t+H_c-1,\\
&\mathbf{y}_{n,t} = \mathbf{h}(\mathbf{x}_{n,t}), \quad n = t+1, \ldots, t+H_p,\\
&\mathbf{x}_{t,t} = \mathbf{x}(t),\\
&\mathbf{u}_{t-1,t} = \mathbf{u}(t-1),\\
&\mathbf{u}_{\min} \le \mathbf{u}_{n,t} \le \mathbf{u}_{\max}, \quad n = t, \ldots, t+N_p-1,\\
&\Delta\mathbf{u}_{\min} \le \Delta\mathbf{u}_{n,t} \le \Delta\mathbf{u}_{\max}, \quad n = t, \ldots, t+N_c-1,\\
&\mathbf{y}_{\min} \le \mathbf{y}_{n,t} \le \mathbf{y}_{\max}, \quad n = t, \ldots, t+N_p-1.
\end{aligned} \tag{31}$$

4.3 Lower level controller design

Based on the target steering angles and the longitudinal tire forces optimized by the upper block in Section 4.2, the lower level block is designed to conduct the target values. Considering the transient characteristics of the steering system, the steering angles can be expressed as follows:

$$\delta_f = \frac{1}{1+\tau_1 s}\delta_{f\_tar}, \ \delta_r = \frac{1}{1+\tau_1 s}\delta_{r\_tar}, \tag{32}$$

where τ_1 is the time constant of the steering system.

To realize the target values of longitudinal tire forces, the brake pressure of ESC can be expressed as follows [30], and an overview of the brake system for each wheel can be expressed as Figure 8.

$$P_{Bfl\_tar} = \frac{R}{K_{Bf}}F_{xfl\_tar}, P_{Bfr\_tar} = \frac{R}{K_{Bf}}F_{xfr\_tar}, \tag{33}$$

$$P_{Brl\_tar} = \frac{R}{K_{Br}}F_{xrl\_tar}, P_{Brr\_tar} = \frac{R}{K_{Br}}F_{xrr\_tar}, \tag{34}$$

where K_{Bf} and K_{Br} are the master cylinder pressure coefficients of the front and rear wheels, respectively.

Considering the transient characteristics of the braking system, eqs. (33) and (34) can be expressed as follows:

$$P_{Bfl} = \frac{1}{1+\tau_2 s}P_{Bfl\_tar}, P_{Bfr} = \frac{1}{1+\tau_2 s}P_{Bfr\_tar}, \tag{35}$$

$$P_{Brl} = \frac{1}{1+\tau_2 s}P_{Brl\_tar}, P_{Brr} = \frac{1}{1+\tau_2 s}P_{Brr\_tar}, \tag{36}$$

where τ_2 represents the time constant of the braking system.

5 Simulation and analysis

Co-simulation on the platform of Carsim and MATLAB is conducted at an initial longitudinal velocity of 72 km/h to verify the effectiveness of the MPC, assuming that the road friction coefficient is 0.8. A D-Class Minivan is applied, whose parameters are detailed in Tables 1 and 2. Other controllers—traditional electronic stability control (T-ESC), which is controlled only by DYC, and an uncontrolled strategy—are compared with the proposed MPC. A sinusoidal input with an amplitude of 120° is shown in Figure 9. The target front and rear steering angles, active front and rear steering angle increments, longitudinal tire forces and brake pressure of the hydraulic cylinder of the MPC are shown in Figure 10. The vehicle responses with different controllers are shown in Figure 11.

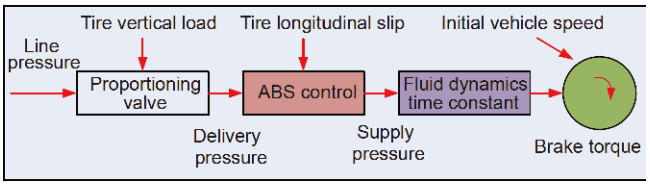

Figure 8 (Color online) Overview of the brake system for each wheel.

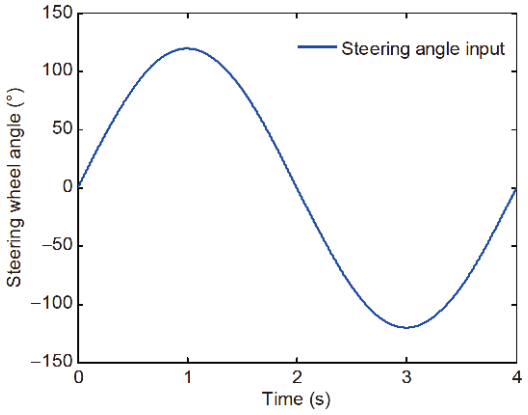

Figure 9 (Color online) Steering angle input of steering wheel.

In this paper, the sample time of the MPC and the T-ESC is 10 ms. The prediction horizon N_p and the control horizon N_c are 20 and 10, respectively. The weight matrices $\mathbf{Q}$ of the controlled outputs of MPC, the weight matrices $\mathbf{R}_1$ of the controlled vectors of MPC, and the weight matrices $\mathbf{R}_2$ of the controlled vectors of T-ESC are set as follows:

$$\mathbf{Q} = \begin{bmatrix} 8\times10^{7} & 0 \\ 0 & 1.8\times10^{5} \end{bmatrix},$$

$$\mathbf{R}_1 = \begin{bmatrix} 150 & 0 & 0 & 0 & 0 & 0 \\ 0 & 10 & 0 & 0 & 0 & 0 \\ 0 & 0 & 1.5\times10^{-3} & 0 & 0 & 0 \\ 0 & 0 & 0 & 1.5\times10^{-3} & 0 & 0 \\ 0 & 0 & 0 & 0 & 1.5\times10^{-3} & 0 \\ 0 & 0 & 0 & 0 & 0 & 1.5\times10^{-3} \end{bmatrix},$$

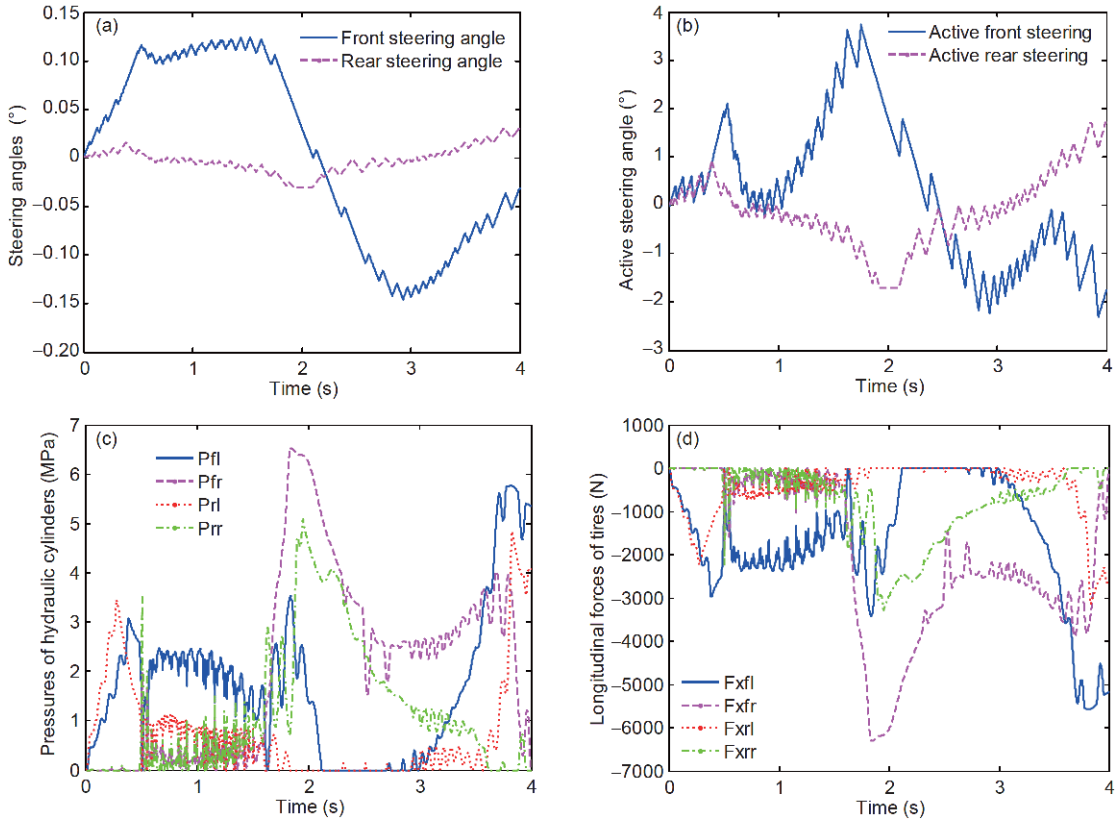

Figure 10 (Color online) Target values of the MPC. (a) Target front and rear steering angles of wheels; (b) active front and rear steering angles of wheels; (c) brake pressures of hydraulic cylinders; (d) target longitudinal forces of each wheel.

Table 2 Major vehicle parameters

Symbols	Parameters	Values
k_f	Cornering stiffness of front axle	−66900 N/rad
k_r	Cornering stiffness of rear axle	−62700 N/rad
K_{Bf}	Transport delayed master cylinder pressure of front wheels	300 N m/MPa
K_{Br}	Transport delayed master cylinder pressure of rear wheels	200 N m/MPa
ρ	Weight of relaxation factor	1000
i	Steering ratio	19.5

$$\mathbf{R}_2 = \begin{bmatrix} 1.5\times10^{-3} & 0 & 0 & 0 \\ 0 & 1.5\times10^{-3} & 0 & 0 \\ 0 & 0 & 1.5\times10^{-3} & 0 \\ 0 & 0 & 0 & 1.5\times10^{-3} \end{bmatrix}.$$

Figure 10 shows the target steering angles, active steering angles, longitudinal tire forces and brake pressures of the wheels. The maximum active steering angle is 3.8° at 2.8 s, as shown in Figure 10(a) and (b). The active front steering angle compensation is positive from 0 to 2.5 s and negative from 2.5 to 4 s, with the intent of turning the vehicle from understeering to neutral steering. In addition, the active rear steering angle is negative from 0 to 2.5 s and positive from 2.5 to 4 s, with the intent of turning the vehicle from understeering to neutral steering. In conclusion, when comparing the active rear steering angle, the active front steering angle is opposite from 0 to 2.5 s and from 2.5 to 4 s, respectively. However, the purposes of the active front and rear steering angle are the same, intending to turn the vehicle from understeering to neutral steering. To control the vehicle from understeering to neutral steering, as with the control effect of the active steering angle, Figure 10(c) and (d) shows that the brake pressures and longitudinal forces of the left wheels are greater than those of the right wheels from 0 to 2 s, and the brake pressures and longitudinal forces of the right wheels are greater than those of the left wheels from 2 to 4 s.

Figure 11 illustrates the results of the vehicle under the different blocks: MPC, T-ESC and without a control strategy. As shown in Figure 11(a), we can conclude that the yaw rates

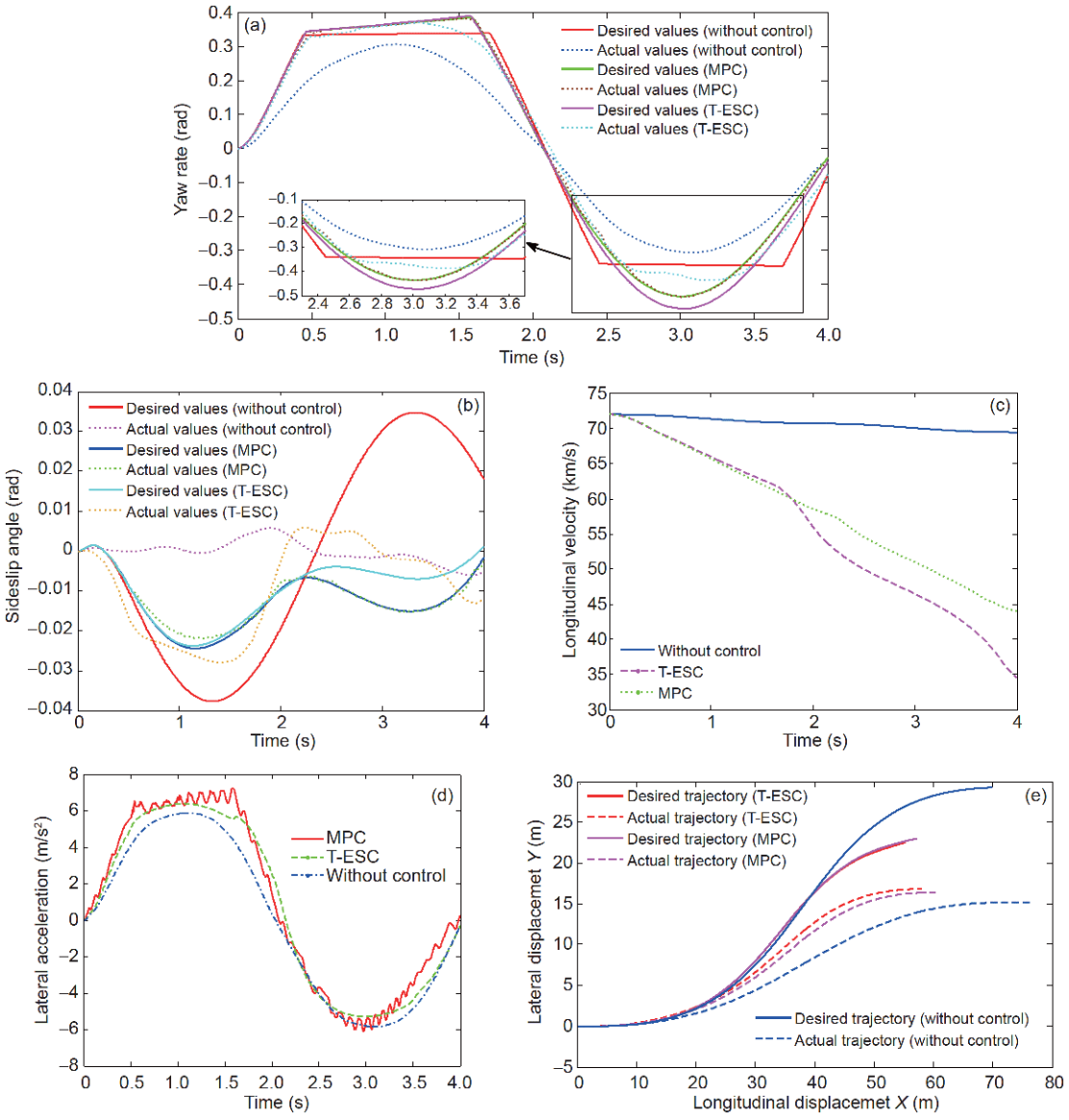

Figure 11 (Color online) Responses of vehicle with different controllers. (a) Yaw rates; (b) sideslip angles; (c) longitudinal velocities; (d) lateral accelerations; (e) vehicle trajectories.

controlled by the MPC and T-ESC can track the desired yaw rates, whereas the yaw rate without a control cannot track the desired value and there are large deviations. Moreover, the yaw rate error controlled by the T-ESC occurs from 2.6–3.4 s, and the maximum error is almost 0.1 rad. However, the yaw rates controlled by MPC can track the desired values effectively, and the error is almost zero. Figure 11(b) illustrates that the desired and actual sideslip angles without control are quite different. In contrast, the sideslip angles controlled by the T-ESC tend to track the desired values, while there are still few deviations. The reason for this phenomenon is that the DYC can control the yaw rate effectively but has less influence on the sideslip angle. Compared to the sideslip angles controlled by the T-ESC, the sideslip angles controlled by MPC can track the desired ones effectively. The results also show that the 4WIS system can compensate for the sideslip angle when the ability to control the sideslip angle of the DYC system has reached its limit. In conclusion, the results shown in Figure 11(a) and (b) illustrate that the MPC developed in the present paper can track the desired yaw rate and sideslip angle effectively, and the control effect is better than T-ESC.

Figure 11(c) shows that the longitudinal velocity controlled by MPC decreases smoothly from 72 to 45 km/h in 4 s, whereas the longitudinal velocity controlled by T-ESC decreases sharply from 72 to 35 km/h in 4 s.

Figure 11(d) shows the results of lateral acceleration with different controllers. As shown in Figure 11(d), we can conclude that the lateral acceleration controlled by T-ESC is greater than that by MPC from 0–2 s. By contrast, the lateral

acceleration controlled by T-ESC is lower than that by MPC from 2–4 s. The reason for this phenomenon is that the longitudinal forces and lateral forces of the MF tire are coupled, and due to the intervention of the active steering system, the longitudinal forces with MPC are lower than those with T-ESC from 2–4 s.

Figure 11(e) shows the vehicle trajectories with different controllers. As shown in Figure 11(e), we can conclude that the tracking effect with the MPC and T-ESC is better than that without a control. We found that the displacement with MPC is longer than that with T-ESC, confirming the conclusions drawn in Figure 11(c) and (e).

To compare the effects of MPC and T-ESC, the error percentage of the longitudinal velocity is defined as follows:

$$\phi = \frac{v_{x0} - v_{xn}}{v_{x0}} \times 100, \tag{37}$$

where v_{x0} and v_{xn} are the initial longitudinal velocity and final longitudinal velocity, respectively.

The control effects of MPC and T-ESC are shown in Table 3. The percentage of longitudinal velocity reduction controlled by T-ESC is 51.4%, whereas the percentage of longitudinal velocity reduction controlled by MPC is 37.5%. Obviously, the influence of the integrated MPC on the longitudinal velocity is reduced by 13.9% in 4 s compared with that of T-ESC. In other words, the MPC proposed in this paper can not only effectively track the desired values but also reduce the effect on longitudinal velocity dramatically compared with T-ESC, providing better longitudinal dynamic performance.

6 Conclusion

Because longitudinal velocity, lateral tire forces and sideslip angle are important state vectors that are not measurable, a UKF observer was designed by utilizing real-time measurements to estimate the longitudinal velocity, lateral tire forces and sideslip angle and then provide accurate values of the required parameters for an upper level controller.

In addition, because DYC has a weak effect on the sideslip angle and always reduces the longitudinal velocity under braking conditions, to simultaneously control the yaw rate and sideslip angle and fully develop the abilities of each system of 4WIS and DYC, an integrated controller of 4WIS and DYC with MPC theory was designed based on the vectors estimated by the UKF observer. To facilitate the MPC design, the MF tire model is simplified based on the Taylor expansion method. A lower level controller is designed to realize the target steering angles and longitudinal tire forces.

Table 3 Control effect comparison

Method	MPC	T-ESC
Initial longitudinal velocity	72 km/h	72 km/h
Final longitudinal velocity	45 km/h	35 km/h
Error percentage	37.5%	51.4%

The results, simulated on the MATLAB/Carsim platform, show that the actual yaw rate and sideslip angle controlled by the MPC could track the desired values, effectively improving the lateral stability. Moreover, the MPC proposed in this paper has less impact on longitudinal velocity compared with T-ESC. The UKF observer can estimate the longitudinal velocity, lateral tire forces and sideslip angle effectively under different road friction coefficient conditions.

In future work, intervention rules will be designed to address the intervention problem of the two systems. According to the different driving states of the vehicle, three intervention rules containing 4WIS, DYC and 4WIS+DYC will be adapted to improve the vehicle stability. In addition, the longitudinal velocity will be considered in the objective function to extremely reduce the influence on the longitudinal dynamics.

This work was supported by the Natural Science Foundation Project of Chongqing (Grant No. cstc2018jcyjAX0077), the Open Fund of Key Laboratory of Advanced Manufacturing Technology for Automobile Parts, Ministry of Education (Grant No. 2018KLMT06), and the Graduate Research and Innovation Foundation of Chongqing, China (Grant No. CYB18059).

1 Li L, Lu Y, Wang R, et al. A three-dimensional dynamics control framework of vehicle lateral stability and rollover prevention via active braking with MPC. IEEE Trans Ind Electron, 2017, 64: 3389–3401
2 Park M, Lee S, Kim M, et al. Integrated differential braking and electric power steering control for advanced lane-change assist systems. P I Mech Eng D-J Aut, 2015, 229: 924–943
3 Cole D J, Pick A J, Odhams A M C. Predictive and linear quadratic methods for potential application to modelling driver steering control. Vehicle Syst Dyn, 2006, 44: 259–284
4 Goharimanesh M, Akbari A A. Improving lateral dynamics of vehicle using direct yaw moment controller based on quantitative feedback theory. Sci Iranica, 2017, 24: 662–672
5 Wen S, Chen M Z Q, Zeng Z, et al. Fuzzy control for uncertain vehicle active suspension systems via dynamic sliding-mode approach. IEEE Trans Syst Man Cybern Syst, 2017, 47: 24–32
6 Furukawa Y, Abe M. Advanced chassis control systems for vehicle handling and active safety. Vehicle Syst Dyn, 1997, 28: 59–86
7 Ding S, Liu L, Zheng W X. Sliding mode direct yaw-moment control design for in-wheel electric vehicles. IEEE Trans Ind Electron, 2017, 64: 6752–6762
8 Ding S, Sun J. Direct yaw-moment control for 4WID electric vehicle via finite-time control technique. Nonlinear Dyn, 2017, 88: 239–254
9 Wu J, Cheng S, Liu B, et al. A human-machine-cooperative-driving controller based on AFS and DYC for vehicle dynamic stability. Energies, 2017, 10: 1737
10 Zhang R H, He Z C, Wang H W, et al. Study on self-tuning tyre friction control for developing main-servo loop integrated chassis control system. IEEE Access, 2017, 5: 6649–6660
11 Heo H, Joa E, Yi K, et al. Integrated chassis control for enhancement of high speed cornering performance. SAE Int J Commer Veh, 2015, 8: 102–109
12 Her H, Joa E, Yi K, et al. Integrated chassis control for optimized tyre

force coordination to enhance the limit handling performance. P I Mech Eng D-J Aut, 2016, 230: 1011–1026
13 Cheng S, Li L, Mei M, et al. Multiple-objective adaptive cruise control system integrated with DYC. IEEE Trans Veh Technol, 2019, 68: 4550–4559
14 Yang X, Wang Z, Peng W. Coordinated control of AFS and DYC for vehicle handling and stability based on optimal guaranteed cost theory. Vehicle Syst Dyn, 2009, 47: 57–79
15 Meng Q, Zhao T, Qian C, et al. Integrated stability control of AFS and DYC for electric vehicle based on non-smooth control. Int J Syst Sci, 2018, 49: 1518–1528
16 Shuai Z, Zhang H, Wang J, et al. Combined AFS and DYC control of four-wheel-independent-drive electric vehicles over CAN network with time-varying delays. IEEE Trans Veh Technol, 2014, 63: 591–602
17 Fan X, Zhao Z. Vehicle dynamics modeling and electronic stability program/active front steering sliding mode integrated control. Asian J Control, 2018, 402: doi: 10.1002/asjc.1822
18 Ding N, Taheri S. An adaptive integrated algorithm for active front steering and direct yaw moment control based on direct Lyapunov method. Vehicle Syst Dyn, 2010, 48: 1193–1213
19 Zhao J, Wong P K, Ma X, et al. Chassis integrated control for active suspension, active front steering and direct yaw moment systems using hierarchical strategy. Vehicle Syst Dyn, 2017, 55: 72–103
20 Baffet G, Charara A, Lechner D, et al. Experimental evaluation of observers for tire-road forces, sideslip angle and wheel cornering stiffness. Vehicle Syst Dyn, 2008, 46: 501–520
21 Baffet G, Charara A, Lechner D. Estimation of vehicle sideslip, tire force and wheel cornering stiffness. Control Eng Pract, 2009, 17: 1255–1264
22 Jin X J, Yin G. Estimation of lateral tire-road forces and sideslip angle for electric vehicles using interacting multiple model filter approach. J Frankl Inst, 2015, 352: 686–707
23 Song Y, Shu H, Chen X, et al. Direct-yaw-moment control of four-wheel-drive electrical vehicle based on lateral tyre-road forces and sideslip angle observer. IET Intelligent Transp Syst, 2019, 13: 303–312
24 Jung H, Choi S B. Real-time individual tire force estimation for an all-wheel drive vehicle. IEEE Trans Veh Technol, 2018, 67: 2934–2944
25 Cheng S, Mei M, Ran X, et al. Adaptive unified monitoring system design for tire-road information. J Dyn Sys Meas Control, 2019, 141: 071006
26 Cheng S, Li L, Chen J. Fusion algorithm design based on adaptive SCKF and integral correction for side-slip angle observation. IEEE Trans Ind Electron, 2017, 65: 5754–5763
27 Jin X J, Yin G, Li Y, et al. Stabilizing vehicle lateral dynamics with considerations of state delay of AFS for electric vehicles via robust gain-scheduling control. Asian J Control, 2016, 18: 89–97
28 Pacejka H B. Tyre and Vehicle Dynamics. 3rd ed. Oxford, Waltham: Butterworth-Heinemann, 2012
29 Julier S J, Uhlmann J K. Unscented filtering and nonlinear estimation. Proc IEEE, 2004, 92: 401–422
30 Yim S. Integrated chassis control with adaptive algorithms. P I Mech Eng D-J Aut, 2016, 230: 1264–1272